Biomineral Coating Increases Bone Formation by Ex Vivo BMP-7 Gene Therapy in Rapid Prototyped Poly(L-lactic acid) (PLLA) and Poly(ε-caprolactone) (PCL) Porous Scaffolds

*Eiji Saito, Darilis Suarez-Gonzalez, William L. Murphy, and Scott J. Hollister**

Porousbiodegradable polymer scaffolds are widely utilized for bone tissue engineering, but are not osteoconductive like calcium phosphate scaffolds. We combine indirect solid freeform fabrication (SFF), ex vivo gene therapy, with biomineral coating to compare the effect of biomineral coating on bone regeneration for Poly (L-lactic acid) (PLLA) and Poly (ε-caprolactone) (PCL) scaffolds with the same porous architecture. Scanning electron microscope (SEM) and micro-computed tomography (μ-CT) demonstrate PLLA and PCL scaffolds have the same porous architecture and are completely coated. All scaffolds are seeded with human gingival fibroblasts (HGF) transduced with adenovirus encoded with either bone morphogenetic protein 7 (BMP-7) or green fluorescent protein (GFP), and implanted into mice subcutaneously for 3 and 10 weeks. Only scaffolds with BMP-7 transduced HGFs show mineralized tissue formation. At 3 weeks some blood vessel-like structures are observed in coated PLLA and PCL scaffolds, but there is no significant difference in bone ingrowth between the coated and uncoated scaffolds for either PLLA or PCL. At 10 weeks, however, coated scaffolds (both PLLA and PCL) have significantly more bone ingrowth than uncoated scaffolds, which have more fibrous tissue. Coated PLLA scaffolds have improved mechanical properties compared with uncoated PLLA scaffolds due to increased bone ingrowth.

1. Introduction

Numerous scaffolds have been investigated for reconstructing bone defects using tissue engineering. Ideal bone tissue engineering scaffolds should be fabricated to fit complex defect shapes and support mechanical loads. Furthermore, they should enhance tissue ingrowth and degrade in conjunction with tissue healing.[1] To achieve these goals, computer-aided design (CAD) and solid freeform fabrication (SFF) or 3D printing techniques have been utilized to fabricate biodegradable scaffolds from various materials and in various shapes.[2–5] SFF scaffolds have well controlled and interconnected pores to enhance cell migration as well as superior mechanical properties for load-bearing applications compared with conventional scaffolds, made from processes such as porogen leaching.[6–9]

FDA-approved biodegradable poly (α-hydroxy esters), including poly (L-lactic acid) (PLLA) and poly(ε-caprolactone) (PCL), have been widely used for orthopedic implants, tissue engineering scaffolds, and drug delivery vehicles.[10–13] It is well known that both materials degrade by hydrolysis, but PCL has a more hydrophobic surface and slower degradation than PLLA.[14,15] In spite of the wide usage of these polymers, one of their disadvantages is poor osteoconductivity compared with scaffolds made of hydroxyapatite (HA) and tricalcium phosphate (TCP).

Biomineral coating of substrate surfaces using simulated body fluid (SBF), which contains similar ion components to human blood, is a promising technique to improve the osteoconductivity of bone tissue engineering scaffolds.[16–18] In this

Dr. E. Saito, Prof. S. J. Hollister
Department of Biomedical Engineering
1101 Beal Ave. University of Michigan
Ann Arbor, MI 48109–2099, USA
E-mail: scottho@umich.edu
Dr. D. Suarez-Gonzalez, Prof. W. L. Murphy
Materials Science Program
University of Wisconsin
Madison, WI 53706, USA
Prof. W. L. Murphy
Department of Biomedical Engineering
University of Wisconsin
Madison, WI 53706, USA
Prof. W. L. Murphy
Department of Orthopedics and Rehabilitation
University of Wisconsin
Madison, WI 53706, USA
Prof. S. J. Hollister
Department of Mechanical Engineering
University of Michigan
Ann Arbor, MI 48109–2125, USA
Prof. S. J. Hollister
Department of Surgery
University of Michigan
Ann Arbor, MI 48109–032, USA

DOI: 10.1002/adhm.201400424

technique, biomaterials are immersed in SBF, and then nanostructured carbonate apatite minerals, similar to the mineral component of bone tissue, precipitate on the biomaterial surfaces.[17,19,20] This method has successfully been applied to various biomaterials including metals,[21,22] polymers,[19,23,24] and the composites of polymers and HA or other calcium phosphate minerals[23,25,26] to enhance bone cell function and bone tissue regeneration. Previous studies show promising effects of biomineral coating including enhanced bone ingrowth and more direct bone surface contact on mineral-coated titanium implants compared to uncoated titanium implants.[21,22,27] A few coated biodegradable substrates, such as PLGA scaffolds and microspheres, have also shown improved bone formation *in vivo*.[28,29]

Although many previous studies have demonstrated a positive effect of apatite-coatings on bone tissue formation, other studies have shown less beneficial effects of mineral coatings. Specifically, some studies found a diminished effect of biomineral coatings on bone formation and fibrovascular tissues, with increased numbers of body giant cells in vivo using porous poly(ε-caprolactone-*co*-L-lactide) scaffolds, SFF PCL scaffolds, or SFF titanium scaffolds.[23,24,30] In addition, mineral-coated scaffolds formed via salt-leaching techniques tend to have less open pore structures that limit effective coating at the center of the scaffolds, resulting in poor bone ingrowth towards the center of the scaffolds.[31] Taken together, these studies suggest a potentially important effect of biomineral-coated biodegradable scaffolds on *in vivo* bone formation, but the effect of scaffold substrate material and porous architecture morphology on the efficacy of biomaterial coating is still not well understood.

In order to develop ideal scaffolds for bone regeneration, it is necessary to understand not only the effect of biomineral coatings on biodegradable scaffolds but also the effect of biomineral-coated scaffolds on different substrate materials with the same porous architecture. To address these needs, we combined SFF scaffolds with biomineral coating using two types of biodegradable polymers, PLLA and PCL. We previously characterized this coating on design 3D printed scaffolds with interconnected pore structures.[32] In the present study, bone tissue was regenerated in ectopic site utilizing bone morphogenetic protein 7 (BMP-7)-transduced human gingival fibroblasts (HGFs) delivered from the scaffolds, a commonly used model for bone tissue engineering.[33–36] We hypothesized that biomineral-coated SFF scaffolds would have improved bone ingrowth over uncoated scaffolds seeded with BMP-7-transduced HGFs, and that the different degradation characteristics of PLLA and PCL would also influence bone ingrowth. PLLA and PCL scaffolds with the same designed porous architecture were fabricated using indirect SFF and coated with a modified SBF technique. The fabricated scaffolds were characterized using micro-computed tomography (μ-CT) and scanning electron microscope (SEM) techniques. Subsequently, the scaffolds were seeded with either BMP-7 or green fluorescent protein (GFP)-transduced HGFs. Finally scaffold/cell constructs were subcutaneously implanted into mice for 3 and 10 weeks. The regenerated bone tissue along with base scaffold materials was characterized using μ-CT, histology. and mechanical testing techniques.

2. Results

2.1. Architecture and Morphology of Coated and Uncoated Scaffolds

The gross images of the fabricated scaffolds are shown in **Figure 1**a–d provided from our previous publication with permission.[32] The uncoated PLLA and PCL scaffolds had similar 3D architecture and surface morphology, which became less transparent after mineral coating. Microscopic architecture, including pore interconnection, of the uncoated PLLA and PCL scaffolds was analyzed using μ-CT (Figure 1f,h). Pore size, strut size, volume, surface area, and surface to volume ratio were similar between the uncoated PLLA and PCL scaffolds, demonstrating the scaffolds had the same architecture (**Table 1**). μ-CT data also showed the existence of mineral layers inside the coated scaffold architectures (Figure 1e,g). A smoother surface was observed on the uncoated PLLA and PCL scaffolds (Figure 1j,l,n,p), while the coated PLLA and PCL scaffolds had a rougher surface (Figure 1i,k,m,o). Nanoscale plate-like crystalline structures were observed in the mineral coating on both coated PLLA and PCL scaffolds (**Figure 2**a,b) provided from our previous publication with permission.[32] Analysis of the biomineral composition by X-ray energy-dispersive spectroscopy (XEDS) showed that the mineral was composed primarily of calcium and phosphorous with a Ca/P ratio of 1.58 for the coated PLLA scaffold (Figure 2 c) and 1.56 for the coated PCL scaffold (Figure 2d), which are both in the range of biological apatites. Biomineral crystallinity, obtained after dissolving the coated PLLA and PCL scaffolds in chloroform, showed that the coated PLLA and PCL scaffolds had mineral crystal peaks similar to those of HA (Figure 2e,f). These data demonstrate growth of bone-like minerals on the scaffold surfaces.

2.2. Bone Formation in Implanted Scaffolds

μ-CT cross-section images of 3 and 10 weeks post subcutaneous implantations are shown in **Figure 3**. The white color indicates either regenerated bone tissue or biomineral coating on the scaffolds, while both PLLA and PCL parts were radiolucent. The scaffolds with BMP-7-transduced HGFs were covered by bone-like tissue and a mineralized shell after 3 and 10 weeks implantation as shown on μ-CT images (Figure 3a,c,e,g,i,k,m,o), while scaffolds with GFP- transduced HGFs did not show bone ingrowth or have a mineralized shell (Figure 3b,d,f,h,j,l,n,p). The coated scaffolds with GFP-transduced HGFs showed biomineral layers on the scaffold surfaces (Figure 3b,d,f,h) at 3 and 10 weeks but no gross evidence of bone formation based on morphology.

Overall bone ingrowth for the scaffolds with BMP-7-transduced HGFs was calculated as the amount of bone in the defined global Region of Interest (Global ROI; see Experimental Section). In the μ-CT images, generated bone tissues have higher density than initially coated biomineral layers. To investigate bone ingrowth into the scaffolds without initial mineral coatings, a ROI with threshold value 1100HU was applied, and the amount of mineral from μ-CT of the preimplanted scaffolds was subtracted from total mineral of the post-implanted

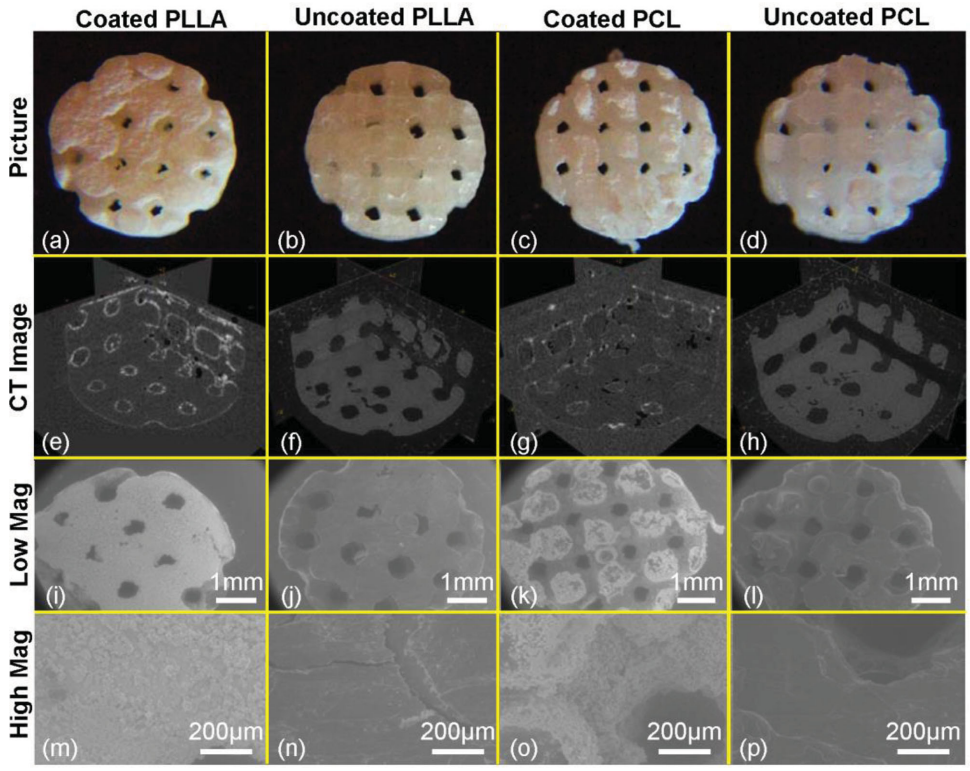

Figure 1. Pictures, μ-CT images, and ESEM images of coated PLLA (a,e,i,m), uncoated PLLA (b,f,j,n), coated PCL (c,g,k,o), and uncoated PCL (d,h,l,p), respectively. μ-CT images confirm that mineral layer covered the surface of both PLLA and PCL scaffolds (e,g). ESEM images show the rough surface of the coated PLLA and PCL scaffolds with low (i,k) and high (m,o) magnifications, while the relatively smooth surface of the uncoated PLLA and PCL scaffolds with low (j,l) and high (n,p) magnifications. Images were provided from our previous study with permission.[32]

scaffolds. As shown in **Figure 4**a–d, there is little bone ingrowth into the scaffold constructs at 3 weeks, and no statistical difference was found between the groups (**Figure 5**a). At 10 weeks, the coated scaffolds had more advanced bone ingrowth than the uncoated scaffolds, and the bone formation followed the architecture of the scaffolds (Figure 4e,g). The uncoated scaffolds showed less bone ingrowth in the scaffolds (Figure 4f,h) at the same time point. Statistical analysis confirmed that coated PLLA and PCL scaffolds had significantly greater bone ingrowth than the uncoated PLLA and PCL scaffolds (Figure 5a, indicated by *). In addition, bone ingrowth of the coated PLLA scaffolds was significantly higher than that of the uncoated PCL scaffolds (Figure 5a, indicated by **), indicating that mineral coating may enhance bone ingrowth over the base material difference.

To further understand bone ingrowth, concentric rings of ROIs (Outermost: ConROI-5, Innermost: ConROI-1, Experimental Section) was applied to the scaffolds at 10 weeks implantation (Figure 5b–e) and the preimplanted scaffolds (Figure 5f). The coated PLLA showed significantly more bone ingrowth than the uncoated PLLA from ConROI-5 to ConROI-2 (Figure 5b, indicated by +), while the coated PCL showed significantly more bone ingrowth than the uncoated PCL from ConROI-4 to ConROI-1 (Figure 5c, indicated by ++). The coated PLLA showed more bone ingrowth than the coated PCL at ConROI-5 (Figure 5d, indicated by +++), while there is no significant difference between the uncoated PLLA and the uncoated PCL (Figure 5e). Although mineral layers were observed over the entire surface of the coated PLLA and PCL scaffolds, the coated PLLA has more initial mineral coating than the coated PCL at ConROI-5, and ConROI-4 (Figure 5f, indicated by #).

2.3. Histology Data

Harvested scaffolds with BMP-7-transduced HGFs were evaluated using histological techniques, H&E (**Figure 6**) and

Table 1. Fabricated uncoated PLLA and PCL scaffolds.

	Pore size [mm]	Strut size [mm]	Volume [mm^3]	Surface [mm^2]	Surface/Volume
PLLA Scaffold	0.60 ± 0.03	0.67 ± 0.03	33.26 ± 2.19	187.13 ± 13.75	5.63 ± 0.20
PCL Scaffold	0.61 ± 0.04	0.67 ± 0.03	30.97 ± 1.29	182.22 ± 10.82	5.88 ± 0.13

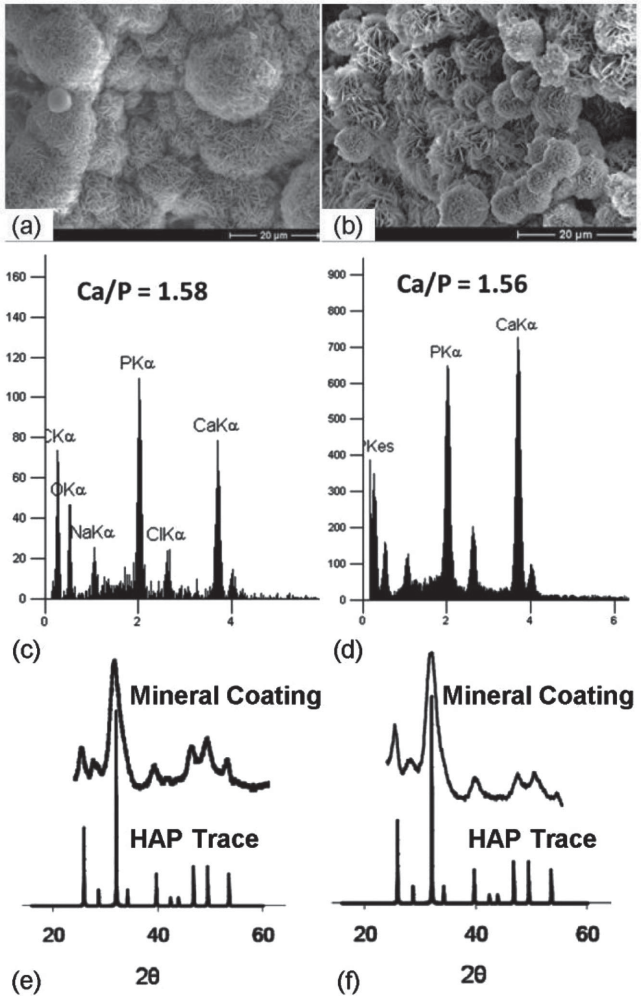

Figure 2. SEM images, XEDS, and XRD data of the coated PLLA (a,c,e) and PCL (b,d,f) scaffolds. SEM images show that nucleated bone-like mineral structures on the coated PLLA (a) and PCL scaffolds (b). XEDS data confirmed that existence of calcium and phosphorous peaks (c,d). XRD data of the mineral- coated scaffolds were obtained after dissolving them in chloroform, coated PLLA (e) and coated PCL (f). Mineral peaks reflecting HAP pattern were shown. Data were provided from our previous study with permission.[32]

Masson's Trichrome (Figure 1, Supporting Information). PLLA and PCL materials were removed by chloroform, and became transparent in the images (indicated by @). H&E staining showed little bone-like tissue formation in the pores of the coated and uncoated PLLA and PCL scaffolds at 3 weeks (Figure 6a,b,e,f). However, the pores of the coated scaffolds contained blood vessel-like tissues, which may be a precursor of bone ingrowth (Figure 6a,e; green arrows). In contrast, the uncoated scaffolds showed few blood vessels (Figure 6b,f). Subsequent 10 week histology of the coated PLLA and PCL scaffolds showed developing bone-like tissue containing marrow in the pores following the pore architecture of the scaffolds (Figure 6c,g). The uncoated PLLA and PCL did not have much bone ingrowth at 10 weeks and contained fibrous-like or fat-like tissues in the pores (Figure 6d,h). Masson's Trichrome staining also showed little bone-like tissue in the pores of coated and uncoated PLLA and PCL scaffolds at 3 weeks (Figure 2a,b,e,f, Supporting Information). At 10 weeks, however, the coated PLLA and PCL scaffolds had well-developed bone tissue containing osteoid (Figure 3c,g, Supporting Information), indicating active deposition of bone mineral in comparison to the uncoated scaffolds.

To investigate the boundary of regenerated bone tissue and initial biomineral coating, the scaffolds with BMP-7-transduced HGFs were embedded in epoxy and sectioned without decalcifying tissues and removing scaffolds (**Figure 7**). Initial mineral coating and regenerated bone tissue was seen on the coated PLLA scaffolds (Figure 7a,e) and the coated PCL scaffolds (Figure 7j,n). Initial mineral coatings show random and less aligned morphology (solid orange arrow) and regenerated bone tissue, while regenerated bone tissue shows more packed and aligned structure (open orange arrow). There was poor bone tissue integration into the mineral coating at 3 weeks (Figure 7, yellow box area (b,k)) as both μ-CT and histological data demonstrate, while bone tissue had more direct bonding on the mineral coating at 10 weeks (Figure 7, yellow box area, left (f,o), and right (g,p). The uncoated PLLA and PCL scaffolds had trabecular-like tissue adjacent to, but not directly integrated to the scaffold surface (Figure 7c,d,l,m), in contrast to the coated scaffold surfaces at 3 weeks. Bone tissue was still lining the scaffold surface (open green arrow) but not integrated into the polymer (solid green arrow) at 10 weeks (Figure 7h,i,q,r), again in contrast to the more intimate bone contact on the coated scaffold surfaces.

2.4. Mechanical Testing of Scaffolds with and Without Bone Tissue

Effective scaffold elastic moduli for the constructs with BMP-7-transduced HGFs were determined at 3 and 10 weeks (**Figure 8**a). The moduli of both coated and uncoated PLLA scaffolds decreased after scaffold implantation from 0 to 3 weeks, likely due to polymer degradation ($p = 0.046$ and 0.001, respectively, indicated by #). The moduli of the coated PLLA scaffolds significantly increased from 3 to 10 weeks ($p = 0.046$, indicated by ##); however, the moduli of uncoated PLLA scaffolds did not significantly increase ($p = 0.590$). Uncoated PCL scaffolds also had significantly increased elastic moduli from 3 to 10 weeks ($p = 0.028$, indicated by ##). Although the coated PCL scaffolds did not have a significant improvement of elastic moduli, the p value was close to the significant level ($p = 0.073$).

Elastic moduli of the scaffolds with GFP-transduced HGFs were also tested (Figure 8b). Only the uncoated PLLA scaffold showed a significant decrease of moduli from 0 to 3 weeks (indicated by +). Moduli of the coated and the uncoated PLLA scaffold increased from 3 to 10 weeks, but not significantly, perhaps due to more fibrous tissue formation resulting from polymer degradation. The coated and uncoated PCL scaffolds show constant moduli throughout the study period indicating little degradation of PCL during this study period.

3. Discussion

Computer-aided tissue engineering utilizing 3D rapid prototyping/3D printing techniques has been used to fabricate

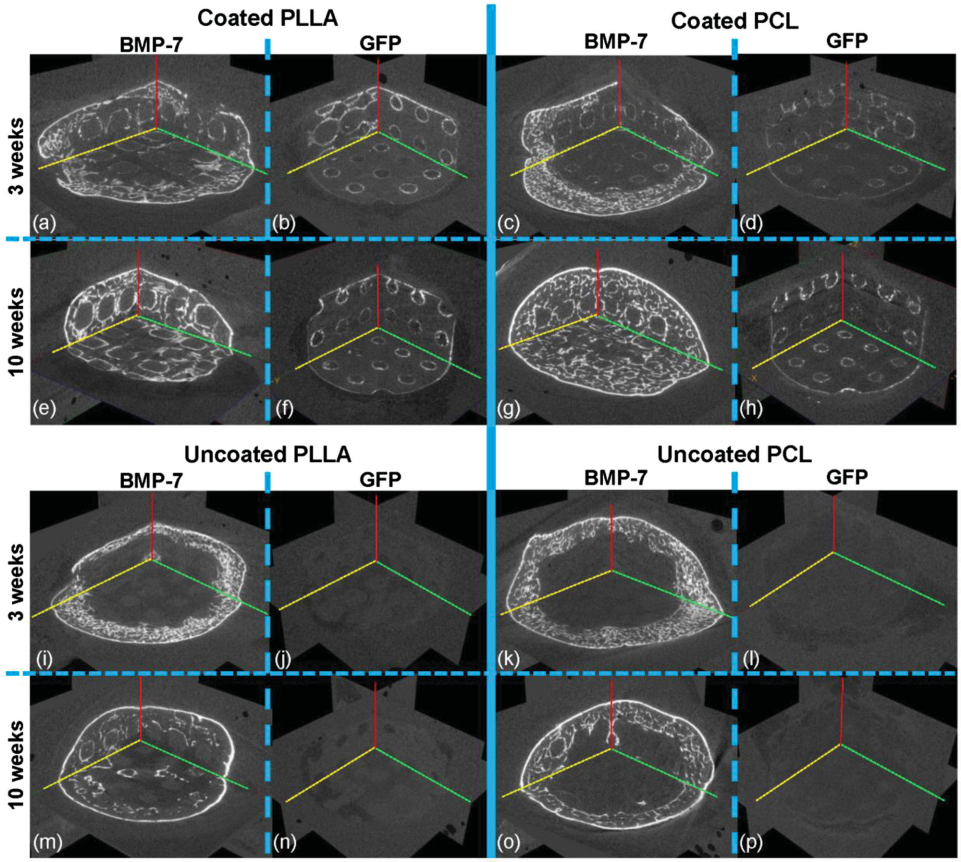

Figure 3. μ-CT cross sectional images of implanted scaffolds with adenovirus BMP-7 or adenovirus GFP-transduced HGFs at 3 and 10 weeks. The scaffolds with BMP-7 groups were covered with bony shells (a,c,e,g,i,k,m,o), while the scaffolds with GFP groups did not show any bony shells (b,d,f,h,j,l,n,p). Coated PLLA and PCL with GFP-transduced scaffolds showed the existence of mineral coating on the scaffold surfaces (b,d,f,h). Uncoated PLLA and PCL with GFP-transduced scaffolds did not appear on the μ-CT images due to low intensity of polymers and no mineralized tissues (j,l,n,p).

scaffolds with precisely controlled architectures matching anatomical shapes and achieving desired properties for clinical applications. These controlled scaffold architectures have been shown to significantly affect both bone formation and scaffold degradation *in vivo*.[37–40] In addition, modified simulated body fluids (mSBF) have been utilized to grow mineral layers on biodegradable materials,[28,41,42] and SFF scaffolds.[43,44] Although some research has investigated the influence of biomineral-coated PLLA and PCL scaffolds on bone regeneration independently,[45,46] no study has successfully investigated the effects of biomineral coatings and scaffold base materials on bone regeneration using identical scaffold porous architectures.

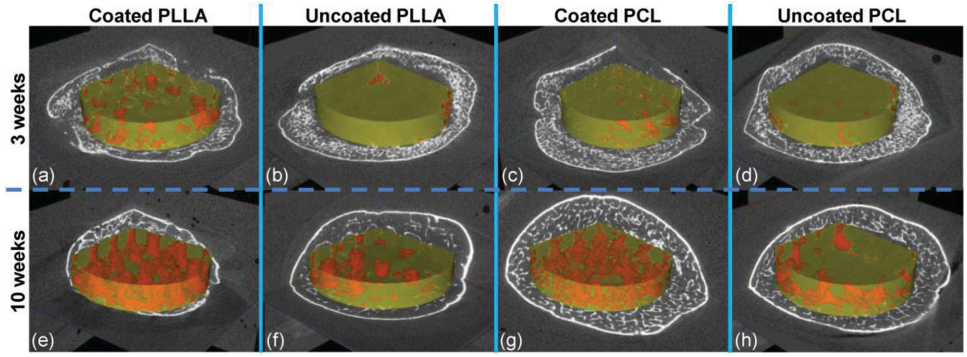

Figure 4. Bone ingrowth into coated PLLA (a,e), uncoated PLLA (b,f), coated PCL (e,g), and uncoated PCL (d,h) scaffolds at 3 and 10 weeks implantation. There was a little bone ingrwoth in the all scaffolds at 3 weeks (a–d). At 10 weeks, the coated PLLA and PCL scaffolds displayed advanced bone ingrowth followed the designed architectures (e,h) compared to the poor bone ingrowth of their respective scaffolds (f,h).

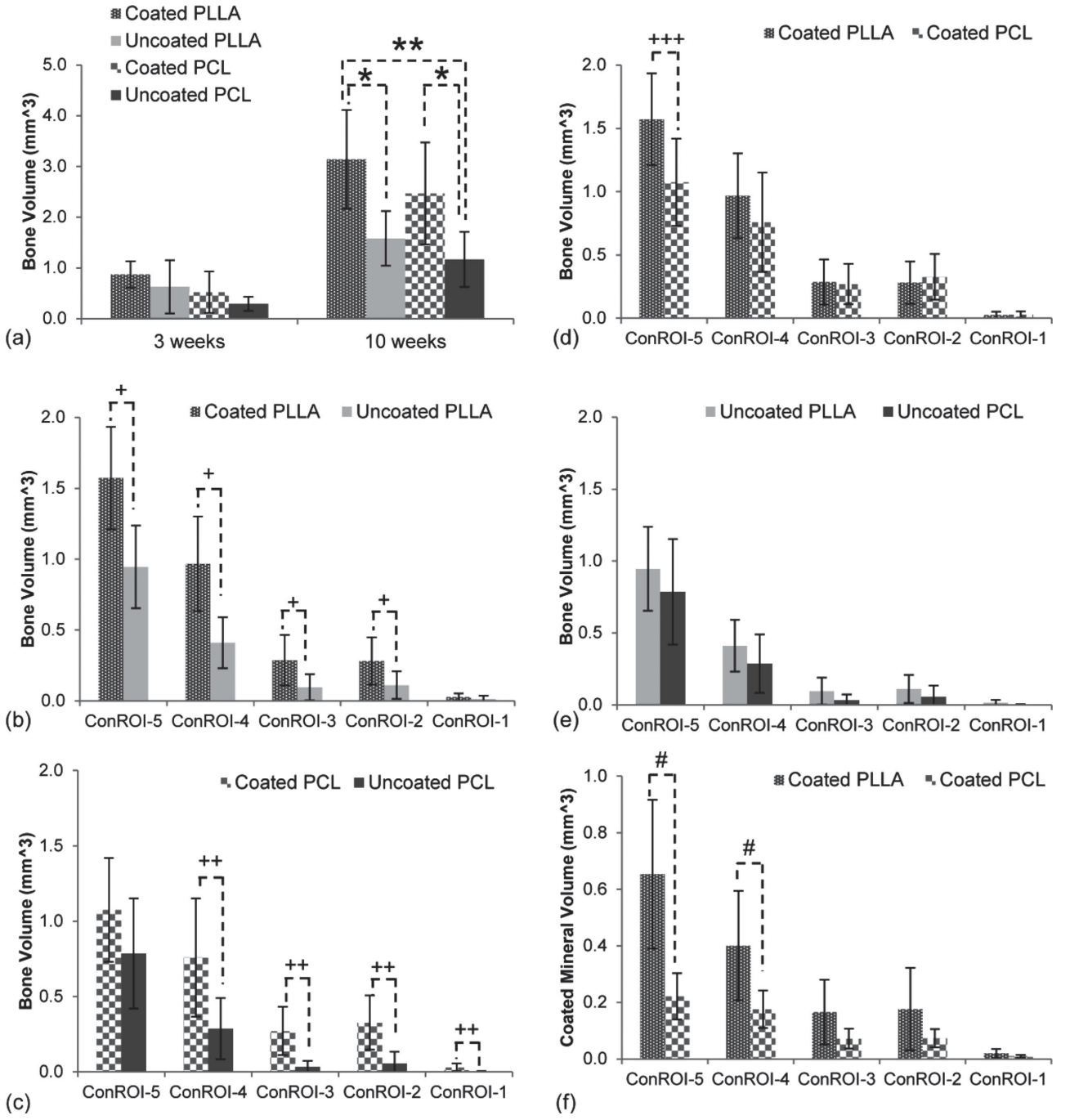

Figure 5. Calculated bone ingrowth (a) in Global ROI at 3 and 10 weeks implantations ($N = 8$). There is no significant difference between the scaffolds at 3 weeks. However, the coated PLLA and PCL scaffolds showed significantly more bone ingrowth than the uncoated PLLA and PCL scaffolds at 10 weeks (indicated by *). In addition, the coated PLLA scaffolds had significantly more bone ingrowth than the uncoated PCL scaffolds at 10 weeks (indicated by **). Concentric ROI was applied to scaffolds at 10 weeks implantation (b–e) and preimplanted scaffolds (f) ($N = 8$). Coated PLLA showed significantly more bone ingrowth than uncoated PLLA with ConROI-5 to -2 (b), while coated PCL showed significantly more bone ingrowth than uncoated PCL with ConROI-4 to -1 (c) (indicated by + and ++, respectively). Coated PLLA showed more bone ingrowth at ConROI-5 than coated PCL (d) (indicated by +++), while there is no significant difference between uncoated PLLA and uncoated PCL (e). Coated PLLA has more initial mineral coating than coated PCL at ConROI-5, and -4 (f) (indicated by #).

Therefore, we developed biomineral-coated PLLA and PCL porous scaffolds combining indirect SFF and mSBF techniques to test the effect of mineral coating and scaffold base materials on *in vivo* bone formation.

The fabricated PLLA and PCL scaffolds were confirmed to have identical structure and orthogonally interconnected channel pores (Figure 1, Table 1), which agreed with our previous SFF scaffold studies including PLLA and PCL

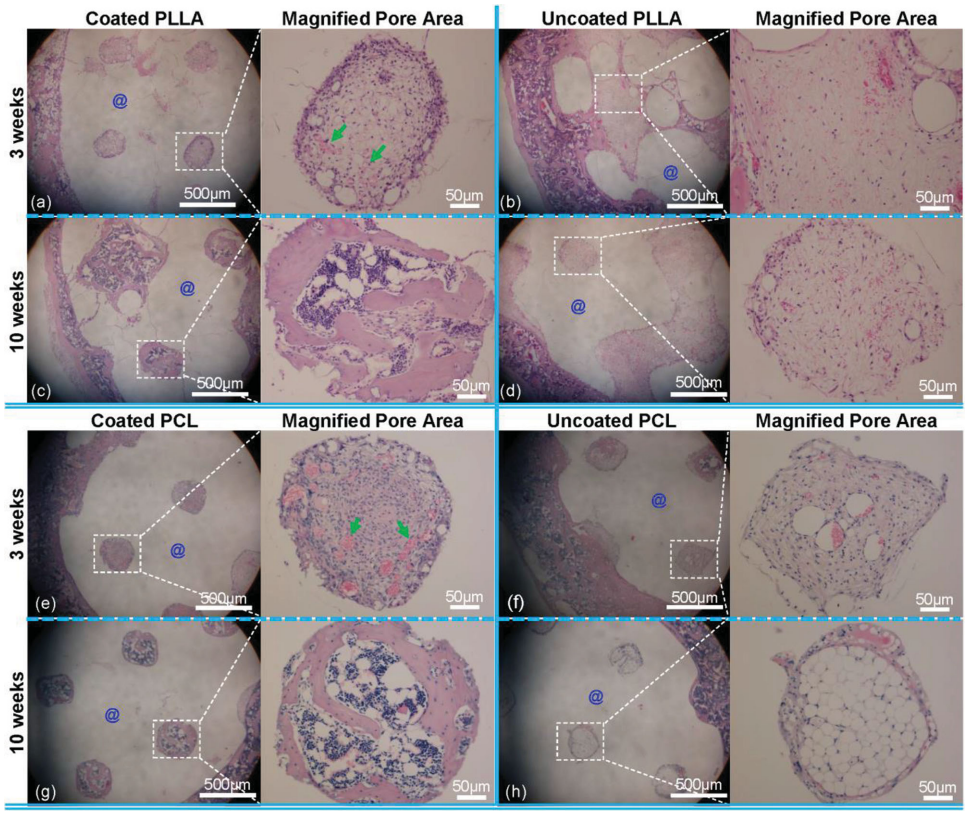

Figure 6. H&E histological staining of implanted PLLA and PCL scaffolds. PLLA and PCL materials were removed and became transparent in the images (indicated by @). Images show little bone ingrowth in the implanted PLLA scaffolds (a,b) and PCL scaffolds (e,f) at 3 weeks. Some blood-vessel-like tissues are observed in the coated PLLA (a) and PCL (e) scaffolds (green arrow), while more fibrous-like tissues are observed in the uncoated PLLA (b) and PCL (f) scaffolds. At 10 weeks, there is well-developed bone ingrowth containing marrow-like tissues in the coated PLLA scaffolds (c) and the coated PCL scaffolds (g), and more fibrous or fat-like tissues in the uncoated PLLA scaffolds (d) and the uncoated PCL scaffolds (h).

scaffolds.[7,38,39] The fact that biomineral layers coved the entire surface of the scaffolds (Figure 1) supports the premise that fully designed interconnected channels of the fabricated scaffolds allowed the mSBF solution to infiltrate into the center of the scaffolds. The coated mineral layers have plate-like morphology, which is similar to human bone tissue, and consistent with biomimetic coating formed in previous studies indicating that the mineral formed in this study is the poorly crystalline, carbonate substituted, and calcium-deficient HA phase.[19,28,44] XEDS data showed calcium and phosphate peaks on the coated mineral, which indicated both coated PLLA and PCL scaffolds had similar nucleated mineral and Ca/P ratios close to that of HA.[19,41]

Ectopic bone formation has been reproducibly generated by delivery of BMP-7-transduced HGFs.[34,47] Bone shells were formed surrounding the scaffolds containing HGF transduced with adenovirus BMP-7, similar to our previous scaffold studies,[36–38,48] whereas control groups with adenovirus GFP-transduced HGFs showed no bone shell formation (Figure 3). The result suggests that bone tissue is mainly induced by secreted BMP-7 proteins, not by biomineral coatings or HGF alone. This is consistent with previous studies demonstrating that biomineral coatings are osteoconductive, but not osteoinductive, that is capable of inducing ectopic bone formation.[49]

Interestingly, the significant effect of biomineral coatings on bone formation was found at 10 week implantation, but not at 3 weeks (Figure 4 and 5a). Previous paper suggest that host mesenchymal stem cells are primarily involved in bone formation, and there is less contribution from transduced cells.[34,47] In addition, most bone formation started outside of the scaffolds. Therefore, 3 weeks may not be long enough for bone forming cells to migrate into the scaffolds to create bone tissue. Once the cells have migrated into the porous area of scaffolds, the existence of the mineral layer encouraged increased bone ingrowth at 10 weeks. The improvement of bone formation by biomineral coatings agreed with some of the previous studies performed using PLGA scaffolds in orthotopic sites[28] and PLGA microspheres in ectopic sites.[29]

Concentric ROI analysis of bone ingrowth suggests that coated scaffold base materials encouraged further penetration of bone interior to the scaffolds (Figure 5b–d). The coated PLLA scaffolds had more bone ingrowth towards the outer edge compared with the coated PCL scaffolds, perhaps due to more initial mineral coating on the coated PLLA scaffolds than the coated PCL scaffolds. The coated PCL showed more bone formation deep inside of the scaffolds than the uncoated PCL scaffolds. Conversely, the coated PLLA scaffolds did not show significant differences at the very inside of the scaffolds compared with the uncoated PLLA scaffolds. We speculate that this may be explained by inhibition of bone formation by PLLA degradation by-products, and slower degradation

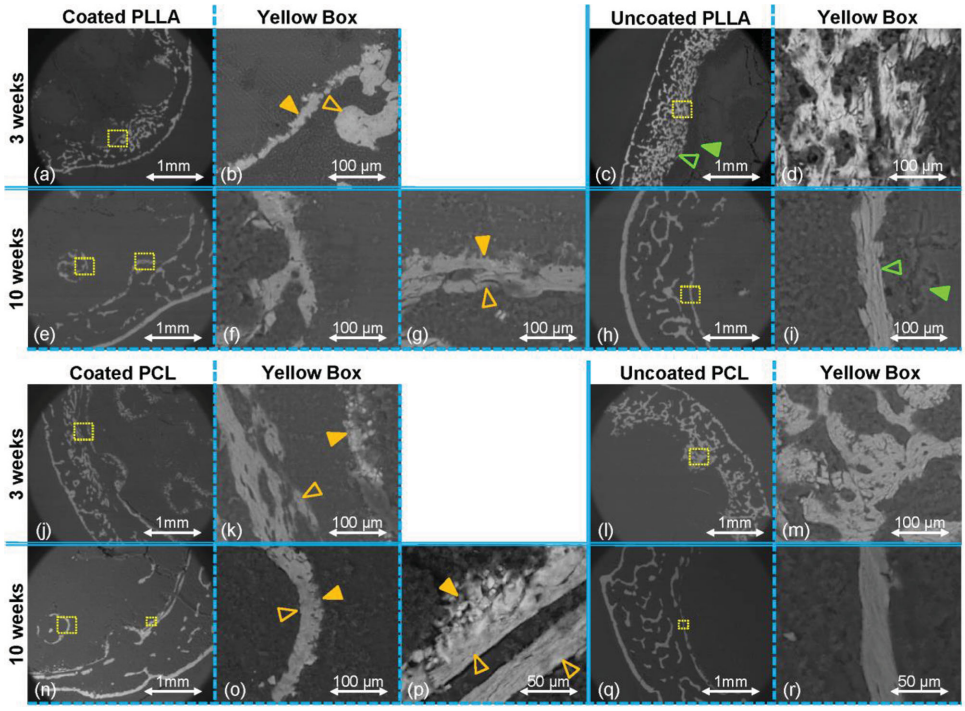

Figure 7. Cross-sectional images of implanted coated PLLA, uncoated PLLA, coated PCL, and uncoated PCL scaffolds at 3 and 10 weeks. Initial mineral coatings and regenerated bone tissues were seen on the coated PLLA scaffolds (a,e) and the coated PCL scaffolds (j,n). There was not clear integration of bone tissues into mineral coatings at 3 weeks (yellow box area (b,k)), while tissues had more bonding on minerals at 10 weeks (yellow box area, left (f,o) and right (g,p)). The arrows show that original mineral coating (solid orange arrow) and regenerated bone tissues (open orange arrow). The uncoated PLLA and PCL scaffolds showed trabecular-like tissues close to the scaffold surface (yellow box (d,m)) at 3 weeks, and lined bone tissue around the scaffold at 10 weeks (yellow box (i,r)). There are some spaces between the generated bone tissue (open green arrow) and the scaffold surface (solid green arrow).

of PCL, which may produce fewer by-products limiting bone formation.[15]

The cross-sections of the biomineral-coated scaffolds showed good bone contact on the biomineral coatings as well as more bone-like tissue formation, indicating that the biomineral coatings supported direct bone formation rather than fibrous tissue formation (Figure 6, 7, 1, Supporting Information).[26,27,29] Furthermore, a significant advantage of combining SFF with biomineralization is demonstrated by regenerated bone completely penetrating the connected regions throughout the porous scaffolds, something more difficult to attain with randomly connected salt-leached scaffolds.[31] Thus, the designed and fully connected pore channels of SFF scaffolds likely allowed fluid infiltration into the center of the scaffolds to support complete biomineral coating (a fluid mediated process) as well as tissue ingrowth.[6,8,9]

Despite the minimal effect of biomineral coatings on bone ingrowth at 3 weeks, the histological images show that coated scaffolds had more blood-vessel-like tissue containing bone marrow compared with the uncoated scaffolds (Figure 6). This may enhance the infiltration of bone-forming cells in the scaffolds, which in part explains the increased bone ingrowth in the coated scaffolds at 10 weeks. The blood-vessel-like tissue in the coated scaffolds may also promote nutrient supply, leading to improved bone ingrowth throughout the scaffolds. As noted above, in an *ex vivo* gene therapy approach like the one used in this study, large bony shells tend to form outside of the scaffolds preventing diffusion of nutrients into the center of the scaffolds.[50] This can also cause accumulation of degradation by-products inside the scaffolds, which could inhibit cell migration and tissue ingrowth. Since coated PLLA showed further bone ingrowth than uncoated PLLA scaffolds (Figure 5), having a biomineral coating on the scaffolds may also help counter these negative effects.[29]

Mechanical testing revealed the effect of the mineral coating process on the different materials (Figure 8). Although both PLLA and PCL scaffolds were treated with NaOH in the same manner to functionalize their surfaces for biomineral coating, only PLLA scaffolds had significantly reduced mechanical properties, suggesting that PLLA degraded due to NaOH treatment.[51] Elastic moduli of implanted scaffolds in this study tended to increase with longer implantation time due to increase of tissue mineral density, similar to our previous studies.[38,39,48] This increase was especially significant for the coated PLLA scaffolds with advancing bone ingrowth compared with the uncoated PLLA whose porous area was filled with either fibrous or fat-like tissues. Although PLLA scaffolds degrade very slowly and maintain their architecture over 20 weeks, we have previously shown that this is a reduction in elastic modulus, mass, and molecular weight with longer implantation time in ectopic sites.[40] In contrast, there is not much difference between the p values of the coated and uncoated PCL scaffolds. These data reflect the fact that PLLA degrades much more rapidly than PCL, thus bone ingrowth in the PLLA scaffold more significantly increases the degraded PLLA stiffness as compared to the intact PCL stiffness.

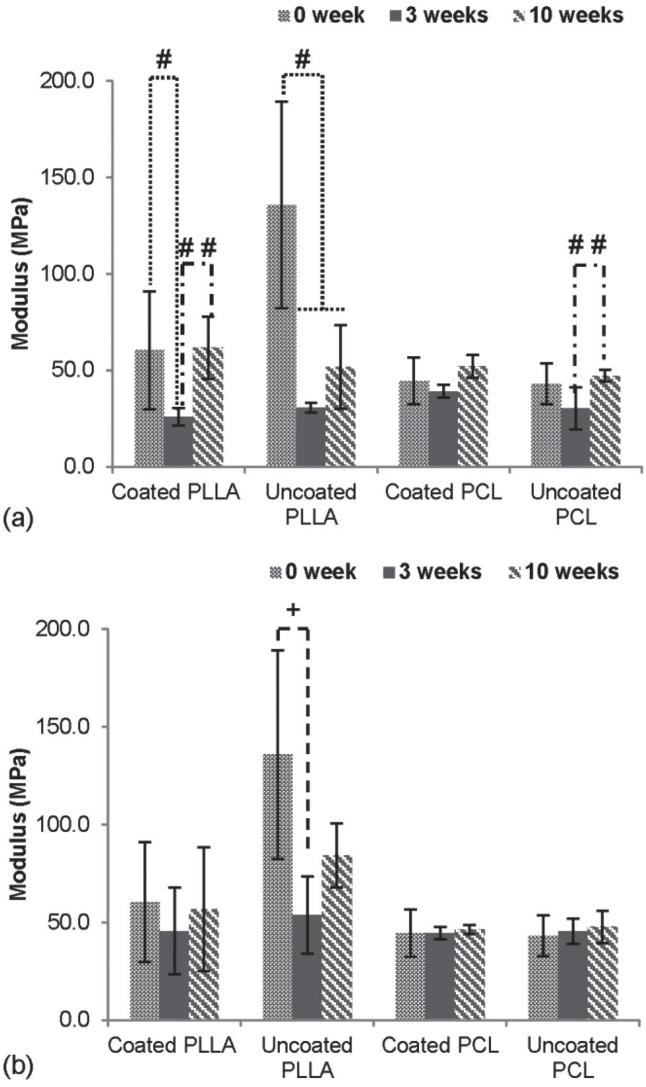

Figure 8. Elastic moduli of the scaffolds with BMP-7-transduced HGFs (a) and with GFP-transduced HGFs (b) (N = 5–6). The coated and uncoated PLLA scaffolds decreased their mechanical properties from 0 to 3 weeks due to the degradation of polymers (indicated by # and +). The mechanical properties of the coated PLLA scaffolds increased significantly from 3 to 10 weeks (indicated by ##), while the uncoated PLLA scaffolds did not have significant increase (a). Both coated and uncoated PCL scaffolds showed a significant (indicated by ##) or close to significant increase of mechanical properties (a).

Our results clearly support the conclusion that biomineral coating improves bone formation, which may be due to several possible mechanisms. The biomineral coating may increase hydrophilicity of PLLA and PCL scaffolds, increasing cell adhesion, migration, and proliferation.[52–54] Calcium phosphate mineral has also been shown to increase protein adsorption, such as fibronectin and vitronectin, which are important for bone cells to adhere on biomaterials and produce extracellular matrices.[55,56] Mineral coatings may also allow for local enrichment of cell-secreted BMP-7 protein, as BMPs are known to interact strongly with biominerals, and the nanostructured biomineral coatings have a large surface area available for BMP binding and release.[44,57] In turn, this local enrichment of BMP-7 may have increased progression of osteogenesis in the mineral-coated scaffolds. Finally, release of calcium ions from biomineral coatings has been reported to promote cell proliferation and differentiation and released calcium may have had a similar effect in our current study.[58] Further mechanistic studies will be required to more definitively delineate the mechanism behind the biomineral coating's effects.

The results of this study are directly relevant to the concept of prefabricated bone flaps, which are constructs placed in an ectopic site in to regenerate bone tissue in preparation for surgical transfer to a bony site, for example to reconstruct complex craniofacial defects. However, examining biomineral-coated scaffolds in orthotopic sites is also important for the development of clinically applicable scaffolds.

4. Conclusion

This study examined the combination of computer-aided engineered scaffolds and biomineral coatings using two biodegradable materials to achieve bone ingrowth into porous scaffolds with identical architectures. SFF scaffolds made of PLLA and PCL were successfully coated with biomineral layers using the same mSBF procedures. The biomineral-coated scaffolds showed improved *in vivo* bone formation, and the resulting bone tissue was fully connected and followed the scaffold pore architectures in contrast to the uncoated scaffolds that had limited bone ingrowth.

5. Experimental Section

Porous Scaffold Design and Fabrication: Porous scaffolds 5 mm in diameter and 3 mm in height with 550 μm pore diameters were designed using image-based techniques and fabricated using the indirect SFF technique.[59,60] The resulting image representations were converted to stereolithography (STL) formats and sliced in Modelworks software (Solidscape, Inc., Merrimack, NH) to fabricate wax molds using a PatternMaster 3D printer (Solidscape, Inc., Merrimack, NH). These wax molds were cast into hydroxyapatite ceramic (HA) secondary molds. Polymer pellets, PLLA (Inherent Viscosity = 0.65 dL g^{-1}, Birmingham Polymers Inc., AL) and PCL (Molecular weight: 43 000–50 000; Polyscience Inc.), were heated at 205 °C and 120 °C, respectively, in a Teflon mold in Lindberg/Blue M Vacuum Oven (Thermo Scientific, Asheville, NC). The HA molds were then placed into the Teflon mold containing molten polymer under vacuum in order to force the polymer through the open pore network. The HA molds were then removed from the porous polymer scaffolds using RDO (APEX Engineering Products Corp, Plainfield, IL) and washed with 100% ethanol.

Mineral Coating Incubation in mSBF: Fabricated PLLA and PCL scaffolds were simultaneously coated in the same manner.[32] The scaffolds were hydrolyzed in a 0.1 M NaOH for 60 min at room temperature to expose carboxylate anions that serve as nucleation sites. After hydrolysis, the scaffolds were rinsed at least three times with deionized H_2O. Each scaffold was incubated at 37 °C in 15 mL of mSBF for 14 d under continuous rotation. The mSBF solution had a similar composition to that of human plasma but with double the concentration of calcium and phosphate, and was prepared as previously reported.[20] Specifically, the following reagents were added to ddH_2O heated to 37 °C in the order shown; 141×10^{-3} M NaCl, 4.0×10^{-3} M KCl, 0.5×10^{-3} M $MgSO_4$, 1.0×10^{-3} M $MgCl_2$, 4.2×10^{-3} M $NaHCO_3$, 20.0×10^{-3} M Tris, 5.0×10^{-3} M $CaCl_2$, and 2.0×10^{-3} M KH_2PO_4. The solution was then adjusted to a final pH of 6.8. The mSBF solution was renewed daily in order to maintain a consistent ionic strength throughout the experiment.

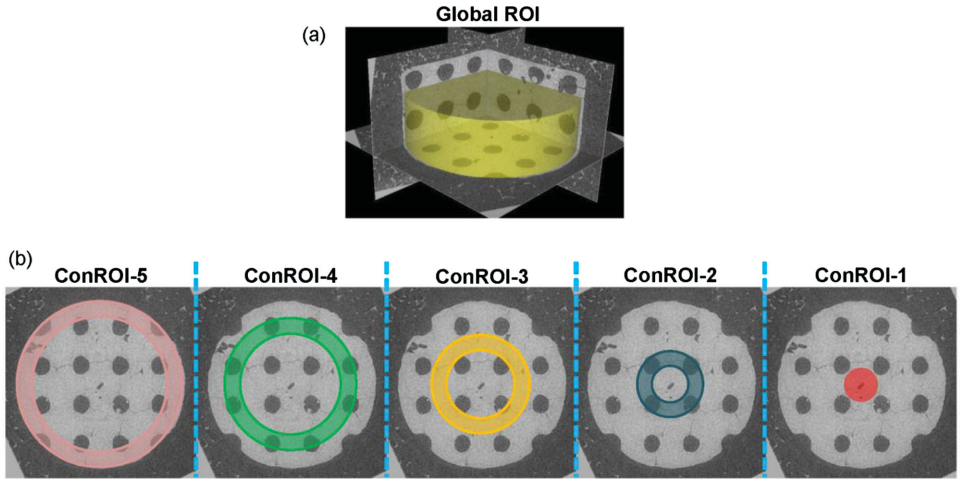

Figure 9. Global ROI was selected with size of 5 mm diameter and 1.8 mm height located within the center of a scaffold, and then a threshold value, 1100, was applied to calculate bone volume (BV) (a). ConROI were applied to 10 weeks data and preimplanted scaffolds by various outer diameter (O.D.) and inner diameter (I.D.) with the same height (1.8 mm), ConROI-5 (O.D. = 5 mm, I.D. = 4 mm), ConROI-4 (O.D. = 4 mm, I.D. = 3 mm), ConROI-3 (O.D. = 3 mm, I.D. = 2 mm), ConROI-2 (O.D. = 2 mm, I.D. = 1 mm), ConROI-1 (O.D. = 1 mm, I.D. = 0 mm) (b). The bone ingrowth was determined by subtracting the amount of mineral in the ROI before implantation from the total amount of mineralized tissue after implantation.

Scaffold Surface Characterization: The surfaces of preimplanted scaffolds were examined in an environmental scanning electron microscope (ESEM), Philips XL30 ESEM. Imaging was performed in variable pressure mode at a pressure of 0.7 Torr and at an accelerating voltage of 10 kV. The coated scaffold surfaces were further investigated using SEM with XEDS. For XRD analysis, the mineral-coated scaffolds were immersed in chloroform (ACROS Organics) and stirred continuously for 20 min or until completely dissolved. The mixture was then centrifuged at 4000 rpm for 5 min to separate out the mineral component. The mineral was rinsed in fresh chloroform and centrifuged for a second time. After collecting the chloroform, the mineral powder was dried under the hood for 2 days to allow residual chloroform to evaporate for XRD analysis. XRD patterns were recorded using a general area detector diffraction system (GADDS), with a Hi-star 2-D area detector ($20° < 2\theta < 40°$) using Cu Kα radiation. The resulting patterns of the samples were identified by computer matching with an International Centre for Diffraction Data (ICDD) powder diffraction database (ICDD card number for HA: 00–001–1008).

Scaffold Implantation in Mice Subcutaneous Sites: Primary HGFs were purchased (ScienCell, CA). HGFs were cultured and expanded on passage 6 near confluence in Dulbecco's modification of Eagles medium (DMEM) supplemented with 10% fetal bovine serum, and 1% penicillin and streptomycin (Gibco). The HGFs were infected with AdCMV-BMP-7, a recombinant adenovirus construct expressing murine BMP-7 gene under a cytomegalovirus (CMV) promoter, or AdCMV-GFP, a recombinant adenovirus construct expressing murine GFP gene under a CMV promoter, at a multiplicity of infection (MOI) of 500 PFU/cell for 20 h. The scaffolds were sterilized in 70% ethanol, washed in Hank's Balanced Salt Solution (Life Technologies), and then in DMEM. 0.5 million cells were seeded into each scaffold by suspending them in 40 µL of 5 mg mL^{-1} collagen gel. The gelation procedure was as follows: Rat tail collagen high concentration (stock concentration = 9.03 mg mL^{-1}; BD Bioscience Discovery Labs, San Jose, CA) were diluted with cold sterile 0.02 N acetic acid to make 5 mg mL^{-1}. As soon as 0.5 N sodium hydroxide with 220 mg mL^{-1} sodium bicarbonate to initiate gelation was added to Col I gel mixture, gel contents were mixed with cell and evenly resuspended. 40 µL of cell and gel mixture was placed in each hole of sterilized custom-made Teflon mold, and the scaffolds were placed on top of gel to enforce infiltration. This was followed by incubation at 37 °C for 40 min to solidify gels further. The scaffolds seeded with HGFs were transferred in ultra-low cluster 24-well plate (Corning Incorporated, NY) with DMEM containing 2% FBS were incubated for 24 h on an orbital shaker. The scaffolds with the transduced HGFs were subcutaneously implanted into 6–7 week old (46–53 days' old) female immunocompromised mice (NIHS-bg-nu-xid, Harlan). After animals were anesthetized with an injection of ketamine/xylazine, 4 subcutaneous pockets were created and 4 scaffolds (one scaffold from each group) were implanted into each mouse. Scaffolds with BMP-7- and GFP-transduced HGFs were implanted into different animals. Finally surgical sites were closed with wound clips in compliance with University Committee on Use and Care of Animal (UCUCA) regulations. The mice were sacrificed at 3 and 10 weeks after the implantation, and the scaffold and tissue constructs were harvested, fixed with Z-fix (Anatech, Battle Creek, MI), and left in 70% ethanol for further assay.

Assay of Scaffolds, Regenerated Tissues, and Amount of Mineral Using µ-CT: All of the scaffolds preimplantation alone and post-implantation with tissue were scanned using a MS-130 high-resolution µ-CT Scanner (GE Medical Systems, Toronto, CAN) at a resolution of 16 µm. The scanned images were reconstructed using MicroView software (GE Healthcare). Each scan was calibrated with a calibration phantom containing air, water, and a material that mimics cortical bone. The calibration values of air and water were set to –1000 and 0 Hounsfield Units (HU), respectively, and the bone HU value was calculated using a standard conversion equation from air and water values.[61] The reconstructed images of the uncoated scaffold prior to implantation were used to calculate pore size, strut size, volume, and surface area, and the reconstructed images of all implanted scaffolds were used to calculate bone ingrowth into porous areas. For bone ingrowth calculations, a global region of interest (Global ROI) was selected with size of 5 mm diameter and 1.8 mm height located within the center of a scaffold, and then a threshold value, 1100 HU, was applied to calculate bone volume (BV) (**Figure 9**a). For further analysis of bone ingrowth, a concentric ROI (ConROI) was applied to both the 10 week data and preimplanted scaffolds by various outer diameters (O.D.) and inner diameters (I.D.) with the same height (1.8 mm), specifically denoted as ConROI-5 (O.D. = 5 mm, I.D. = 4 mm), ConROI-4 (O.D. = 4 mm, I.D. = 3 mm), ConROI-3 (O.D. = 3 mm, I.D. = 2 mm), ConROI-2 (O.D. = 2 mm, I.D. = 1 mm), ConROI-1 (O.D. = 1 mm, I.D. = 0 mm) (Figure 9b). The bone ingrowth was determined by subtracting the amount of mineral in the ROI before implantation from the total amount of mineralized tissue after implantation ($N = 8$). To determine the amount of mineral on the scaffold surfaces, a cylindrical region of interest (ROI) with 5.6 mm diameter and 3.5 mm height was chosen to encompass the whole scaffold, and

then the amount of mineral was calculated applying various threshold, 600 HU, based on our previous studies ($N = 8$).[32]

Mechanical Testing of Scaffolds with Regenerated Tissue: Following μ-CT scanning, compression tests were performed after scaffolds underwent a series of ethanol and were rehydrated in Milli-Q water for 30 min, using an MTS Alliance RT30 Electromechanical test frame (MTS Systems Corp., MN). The heights of the scaffolds were measured with a caliper. The cross-head speed was 1 mm min^{-1} after a preload of 0.227 kg (0.5 lbs). TestWorks4 software (MTS Systems Corp., MN) was used to record load and displacement data. The stress–strain curves were calculated from the initial dimensions of specimens. The compressive modulus was defined by the slope at the initial linear section of the stress–strain curve ($N = 5$–6).

Histological Analysis: After μ-CT scanning, one harvested scaffold from each group was processed for histology. The scaffold and tissue constructs were demineralized with RDO and the residual polymer in the tissue was removed using chloroform prior to paraffin-embedding. The scaffolds were then sectioned at the middle point at 5 μm and stained with hematoxylin and eosin (H&E) and Masson's Trichrome. The implanted scaffolds without decalcification or polymer removal were embedded in epoxy block (Embed 812, Electron Microscopy Sciences) and sectioned with microtome using a diamond blade (Isomet, Buehler, USA) to 200–300 μm thickness.[62] The cross sections were observed in backscattered electron imaging mode in a FEI Quanta focused ion beam workstation and environmental SEM, at a pressure of 0.5 Torr and at an accelerating voltage of 30 kV.

Statistical Analysis: Statistical analysis was performed with SPSS (SPSS, Inc., Chicago, IL USA). Two groups were analyzed with Student's *t*-test for independent samples. Multiple comparison procedures were determined by one-way ANOVA followed by Tukey's Post Hoc multiple comparisons. Standard deviation (SD) was reported in figures, and significance was determined using a probability value of $p < 0.05$.

Supporting Information

Supporting Information is available from the Wiley Online Library or from the author.

Acknowledgements

W.L.M. is a co-founder and shareholder in Tissue Regeneration Systems, Inc. This study was supported by the National Institute of Health (NIH) R01 grant AR 053379 and R21 grant DE 022439. The authors also thank Prof. William Giannobile and Prof. Junro Yamashita in School of Dentistry, and Dr. Claire Jeong in Department of Biomedical Engineering at the University of Michigan for their supply of embedding reagents, use of the microtome and technical supports, and Prof. Paul Krebsbach in School of Dentistry at the University of Michigan for supply of GFP virus. The authors acknowledge Prof. Steve Goldstein's lab at the University of Michigan for their kindness of use of the micro-CT systems.

Received: July 21, 2014
Published online: December 16, 2014

[1] D. W. Hutmacher, *J. Biomater. Sci. Polym. Ed.* **2001**, *12*, 107.
[2] W. Sun, B. Starly, A. Darling, C. Gomez, *Biotechnol. Appl. Biochem.* **2004**, *39*, 49.
[3] D. W. Hutmacher, M. Sittinger, M. V. Risbud, *Trends Biotechnol.* **2004**, *22*, 354.
[4] S. J. Hollister, *Nat. Mater.* **2005**, *4*, 518.
[5] A. Martins, S. Chung, A. J. Pedro, R. A. Sousa, A. P. Marques, R. L. Reis, N. M. Neves, *J. Tissue Eng. Regen. Med.* **2009**, *3*, 37.
[6] F. P. Melchels, A. M. Barradas, C. A. van Blitterswijk, J. de Boer, J. Feijen, D. W. Grijpma, *Acta Biomater.* **2010**, *6*, 4208.
[7] E. Saito, H. Kang, J. M. Taboas, A. Diggs, C. L. Flanagan, S. J. Hollister, *J. Mater. Sci. Mater. Med.* **2010**, *21*, 2371.
[8] K. W. Lee, S. Wang, M. Dadsetan, M. J. Yaszemski, L. Lu, *Biomacromolecules* **2010**, *11*, 682.
[9] K. Kim, D. Dean, J. Wallace, R. Breithaupt, A. G. Mikos, J. P. Fisher, *Biomaterials* **2011**, *32*, 3750.
[10] J. C. Middleton, A. J. Tipton, *Biomaterials* **2000**, *21*, 2335.
[11] R. Morent, N. De Geyter, T. Desmet, P. Dubruel, C. Leys, *Plasma Proc. Polym.* **2011**, *8*, 171.
[12] M. H. Smith, C. L. Flanagan, J. M. Kemppainen, J. A. Sack, H. Chung, S. Das, S. J. Hollister, S. E. Feinberg, *Int. J. Med. Robot.* **2007**, *3*, 207.
[13] D. W. Hutmacher, S. Cool, *J. Cell. Mol. Med.* **2007**, *11*, 654.
[14] D. Hutmacher, M. B. Hurzeler, H. Schliephake, *Int. J. Oral Maxillofac. Implants* **1996**, *11*, 667.
[15] K. Rezwan, Q. Z. Chen, J. J. Blaker, A. R. Boccaccini, *Biomaterials* **2006**, *27*, 3413.
[16] Y. F. Chou, W. Huang, J. C. Dunn, T. A. Miller, B. M. Wu, *Biomaterials* **2005**, *26*, 285.
[17] J. D. Kretlow, A. G. Mikos, *Tissue Eng.* **2007**, *13*, 927.
[18] Y. Liu, G. Wu, K. de Groot, *J. R. Soc. Interface* **2010**, *7*, S631.
[19] W. L. Murphy, D. J. Mooney, *J. Am. Chem. Soc.* **2002**, *124*, 1910.
[20] D. Suarez-Gonzalez, K. Barnhart, E. Saito, R. Vanderby Jr, S. J. Hollister, W. L. Murphy, *J. Biomed. Mater. Res. A.* **2010**, *95*, 222.
[21] F. Barrere, C. M. van der Valk, G. Meijer, R. A. Dalmeijer, K. de Groot, P. Layrolle, *J. Biomed. Mater. Res. B. Appl. Biomater.* **2003**, *67*, 655.
[22] P. Li, *J. Biomed. Mater. Res. A.* **2003**, *66*, 79.
[23] H. Chim, D. W. Hutmacher, A. M. Chou, A. L. Oliveira, R. L. Reis, T. C. Lim, J. T. Schantz, *Int. J. Oral Maxillofac. Surg.* **2006**, *35*, 928.
[24] J. Holmbom, A. Sodergard, E. Ekholm, M. Martson, A. Kuusilehto, P. Saukko, R. Penttinen, *J. Biomed. Mater. Res. A.* **2005**, *75*, 308.
[25] S. S. Kim, M. S. Park, S. J. Gwak, C. Y. Choi, B. S. Kim, *Tissue Eng.* **2006**, *12*, 2997.
[26] D. Lickorish, L. Guan, J. E. Davies, *Biomaterials* **2007**, *28*, 1495.
[27] M. Nagano, T. Kitsugi, T. Nakamura, T. Kokubo, M. Tanahashi, *J. Biomed. Mater. Res.* **1996**, *31*, 487.
[28] W. L. Murphy, C. A. Simmons, D. Kaigler, D. J. Mooney, *J. Dent. Res.* **2004**, *83*, 204.
[29] S. W. Kang, H. S. Yang, S. W. Seo, D. K. Han, B. S. Kim, *J. Biomed. Mater. Res. A.* **2008**, *85*, 747.
[30] M. A. Lopez-Heredia, J. Sohier, C. Gaillard, S. Quillard, M. Dorget, P. Layrolle, *Biomaterials* **2008**, *29*, 2608.
[31] C. Du, G. J. Meijer, C. van de Valk, R. E. Haan, J. M. Bezemer, S. C. Hesseling, F. Z. Cui, K. de Groot, P. Layrolle, *Biomaterials* **2002**, *23*, 4649.
[32] E. Saito, D. Suarez-Gonzalez, R. R. Rao, J. P. Stegemann, W. L. Murphy, S. J. Hollister, *Tissue Eng. Part C. Methods* **2013**, *19*, 507.
[33] P. H. Krebsbach, K. Gu, R. T. Franceschi, R. B. Rutherford, *Hum. Gene Ther.* **2000**, *11*, 1201.
[34] R. B. Rutherford, B. Nussenbaum, P. H. Krebsbach, *Drug News Perspect.* **2003**, *16*, 5.
[35] R. M. Schek, E. N. Wilke, S. J. Hollister, P. H. Krebsbach, *Biomaterials* **2006**, *27*, 1160.
[36] J. M. Williams, A. Adewunmi, R. M. Schek, C. L. Flanagan, P. H. Krebsbach, S. E. Feinberg, S. J. Hollister, S. Das, *Biomaterials* **2005**, *26*, 4817.
[37] A. G. Mitsak, J. M. Kemppainen, M. T. Harris, S. J. Hollister, *Tissue Eng. Part A.* **2011**, *17*, 1831.
[38] S. M. Roosa, J. M. Kemppainen, E. N. Moffitt, P. H. Krebsbach, S. J. Hollister, *J. Biomed. Mater. Res. A.* **2010**, *92*, 359.

[39] E. Saito, E. E. Liao, W. W. Hu, P. H. Krebsbach, S. J. Hollister, *J. Tissue Eng. Regen. Med.* **2013**, *7*, 99.
[40] E. Saito, Y. Liu, F. Migneco, S. J. Hollister, *Acta Biomater.* **2012**.
[41] L. Jongpaiboonkit, T. Franklin-Ford, W. L. Murphy, *ACS Appl. Mater. Interfaces* **2009**, *1*, 1504.
[42] W. L. Murphy, S. Hsiong, T. P. Richardson, C. A. Simmons, D. J. Mooney, *Biomaterials* **2005**, *26*, 303.
[43] M. T. Arafat, C. X. Lam, A. K. Ekaputra, S. Y. Wong, X. Li, I. Gibson, *Acta Biomater.* **2011**, *7*, 809.
[44] D. Suarez-Gonzalez, K. Barnhart, F. Migneco, C. Flanagan, S. J. Hollister, W. L. Murphy, *Biomaterials* **2012**, *33*, 713.
[45] J. Chen, B. Chu, B. S. Hsiao, *J. Biomed. Mater. Res. A.* **2006**, *79*, 307.
[46] J. V. Araujo, A. Martins, I. B. Leonor, E. D. Pinho, R. L. Reis, N. M. Neves, *J. Biomater. Sci. Polym. Ed.* **2008**, *19*, 1261.
[47] R. B. Rutherford, M. Moalli, R. T. Franceschi, D. Wang, K. Gu, P. H. Krebsbach, *Tissue Eng.* **2002**, *8*, 441.
[48] C. Y. Lin, R. M. Schek, A. S. Mistry, X. Shi, A. G. Mikos, P. H. Krebsbach, S. J. Hollister, *Tissue Eng.* **2005**, *11*, 1589.
[49] J. W. Vehof, P. H. Spauwen, J. A. Jansen, *Biomaterials* **2000**, *21*, 2003.
[50] M. C. Kruyt, W. J. Dhert, F. C. Oner, C. A. van Blitterswijk, A. J. Verbout, J. D. de Bruijn, *Biomaterials* **2007**, *28*, 1798.
[51] D. Cam, S. H. Hyon, Y. Ikada, *Biomaterials* **1995**, *16*, 833.
[52] J. V. Araujo, C. Cunha-Reis, T. Rada, M. A. da Silva, M. E. Gomes, Y. Yang, N. Ashammakhi, R. L. Reis, A. J. El-Haj, N. M. Neves, *Tissue Eng. Part A* **2010**, *16*, 557.
[53] Y. Chen, A. F. Mak, M. Wang, J. S. Li, M. S. Wong, *J. Mater. Sci., Mater. Med.* **2008**, *19*, 2261.
[54] M. Ngiam, S. Liao, A. J. Patil, Z. Cheng, F. Yang, M. J. Gubler, S. Ramakrishna, C. K. Chan, *Tissue Eng. Part A* **2009**, *15*, 535.
[55] F. Barrere, C. A. van Blitterswijk, K. de Groot, *Int. J. Nanomed.* **2006**, *1*, 317.
[56] H. S. Yu, J. H. Jang, T. I. Kim, H. H. Lee, H. W. Kim, *J. Biomed. Mater. Res. A.* **2009**, *88*, 747.
[57] J. S. Lee, D. Suarez-Gonzalez, W. L. Murphy, *Adv Mater.* **2011**, *23*, 4279.
[58] J. Wang, J. de Boer, K. de Groot, *J. Biomed. Mater. Res. A* **2009**, *90*, 664.
[59] J. M. Taboas, R. D. Maddox, P. H. Krebsbach, S. J. Hollister, *Biomaterials* **2003**, *24*, 181.
[60] S. J. Hollister, R. A. Levy, T. M. Chu, J. W. Halloran, S. E. Feinberg, *Int. J. Oral Maxillofac. Surg.* **2000**, *29*, 67.
[61] J. A. Meganck, K. M. Kozloff, M. M. Thornton, S. M. Broski, S. A. Goldstein, *Bone* **2009**, *45*, 1104.
[62] P. C. Chang, Y. J. Seol, J. A. Cirelli, G. Pellegrini, Q. Jin, L. M. Franco, S. A. Goldstein, L. A. Chandler, B. Sosnowski, W. V. Giannobile, *Gene Ther.* **2010**, *17*, 95.